The effect of the protein corona on the interaction between nanoparticles and lipid bilayers

Desirè Di Silvio[a,b1] *Marco Maccarini,*[c *] *Roger Parker,*[b] *Alan Mackie,*[b2] *Giovanna Fragneto*[d] *and Francesca Baldelli Bombelli*[e*]

[a] School of Pharmacy, University of East Anglia, Norwich Research Park, Norwich NR4 7TJ, United Kingdom

[b] Institute of Food Research, Norwich Research Park, Colney, Norwich, NR4 7UA, United Kingdom

[c] Univ. Grenoble Alpes - Laboratoire TIMC/IMAG UMR CNRS 5525, Pavillon Taillefer Domaine de la merci, 38700 La Tronche, France

[d] Institut Laue-Langevin, 71 avenue des Martyrs, BP 156 38000, Grenoble, France.

[e] Department of Chemistry, Materials and Chemical Engineering "G. Natta", Politecnico di Milano, Via Mancinelli 7, 20131 Milan, Italy (present affiliation)

Corresponding Author

* marco.maccarini@univ-grenoble-alpes.fr; Phone +33 (0)4 56 52 00 94

*francesca.baldelli@polimi.it; Phone +390223994745

ABSTRACT

[1] Centro de Investigación Cooperativa en Biomateriales CIC biomaGUNE, Paseo Miramon 182, 20009 San Sebastian, Gipuzkoa, Spain.

[2] School of Food Science and Nutrition, University of Leeds, Leeds, LS29JT, UK.

Hypothesis

It is known that nanoparticles (NPs) in a biological fluid are immediately coated by a protein corona (PC), composed of a hard (strongly bounded) and a soft (loosely associated) layers, which represents the real nano-interface interacting with the cellular membrane *in vivo*. In this regard, supported lipid bilayers (SLB) have extensively been used as relevant model systems for elucidating the interaction between biomembranes and NPs. Herein we show how the presence of a PC on the NP surface changes the interaction between NPs and lipid bilayers with particular care on the effects induced by the NPs on the bilayer structure.

Experiments

In the present work we combined Quartz Crystal Microbalance with Dissipation Monitoring (QCM-D) and Neutron Reflectometry (NR) experimental techniques to elucidate how the NP-membrane interaction is modulated by the presence of proteins in the environment and their effect on the lipid bilayer.

Findings

Our study showed that the NP-membrane interaction is significantly affected by the presence of proteins and in particular we observed an important role of the soft corona in this phenomenon.

KEYWORDS

supported lipid bilayer, protein corona nanoparticles, quartz crystal microbalance, neutron reflectometry, soft corona, hard corona.

ABBREVIATION

NPs nanoparticles; SLB supported lipid bilayer; PC protein corona; QCM-D quartz crystal microbalance with dissipation; NR neutron reflectometry; PS polystyrene; PBS phosphate buffered saline; FBS fetal bovine serum; HC hard corona; SC soft corona; DOPC 1,2-Dioleoyl-sn-glycero-3-phosphocholine; SLD scattering length density; APM area per molecule; 4MW 4 matching water; SMW silicon matching water; LUV large unilamellar vesicle; GUV giant unilamellar vesicle; DPPC Dipalmitoyl-phosphatidyl-choline.

1. Introduction

The fast development of nanotechnology and its growing use in different areas in everyday life has highly increased the chances of voluntary or accidental exposure of the human body to nanoparticles (NPs), which in some cases can lead to adverse effects for health. Thus, a clear understanding of the interaction between NPs and biological matter is crucial, independently of the NP final use and not limited to nanomaterials specifically developed for biomedical applications. The first contact between NPs and living organisms occurs at the level of the cell membrane, thus understanding this interaction is a critical step to design safer and more efficient NPs as well as to predict possible toxicity effects.[1-3] Studying these interactions is a challenging topic due to the complexity and heterogeneity of the cell membrane.[1,4] Simpler models representative of the biological membranes provide a useful tool to perform focused studies and unravel the physical and chemical nature of NP-membrane interactions.[3] In fact, model membranes are versatile systems whose composition and structure can be precisely controlled and customized capturing essential aspects of the real membranes, without the influence of cell metabolism and growth.[5] Moreover, model membranes allow the use of a wide range of powerful techniques, like quartz crystal microbalance and scattering techniques, that would be hardly applicable to real membranes.[2]

Supported lipid bilayers (SLBs) represent one of the most used and versatile models for biological membranes. They are planar and can be easily formed by deposition and collapse of vesicles on interfaces with defined surface area.[6] It has been shown that non-specific interactions with the NPs can alter SLB structure and elasticity.[5] NPs can adhere to the lipid bilayer and cause changes in the lipid phase,[7] induce formation of lipid domains[8-9] or pores and extract lipids[10] inducing lipid bilayer disruption.[11-12] Physical chemical properties of NPs,[5,13] such as size,[4, 11, 14-15] charge[12, 16] and surface chemistry[17-20] are the main factors modulating NP-membrane interactions. The same factors are also known to influence the formation of a protein corona (PC) around the NPs in biological fluids.[21] The PC spontaneously forms upon exposure to proteins and consists of multiple layers that have different affinities to the NP surface, in particular the soft corona is defined as the external layer of proteins weakly interacting with the NP, while the hard corona is the most internal protein shell that strongly adheres to the NP surface.[21] Moreover, recently it has been introduced the concept of "personalized protein corona". Not only external factors like temperature, ionic strength, protein concentration and fluid composition, but also characteristics of the patient such as gender, pathology, age, background and lifestyle strongly influence the PC

composition.[22] Since the PC affects the properties of the NP surface, it has significant impact on the interaction between membrane and NPs.[23-27] Many studies are described in the literature where NP cellular uptake is related to the presence of a PC on the NPs in biological fluids,[28-30] in particular it has been shown that a key factor in NPs cellular uptake is their adhesion to the cell membrane that significantly affects their final uptake rates.[31] NP-cell membrane interaction is a complex dynamic process in which the environmental proteins are known to play an important multifaceted role: not only they adsorb onto the NP surface forming the PC, but also they compete with the NP in the interaction with the cell membrane.

Recently, Luchini and co-workers,[32] reported the use of neutron reflectometry (NR) and quartz crystal microbalance with dissipation monitoring (QCM-D) to elucidate the interactions between iron oxide NPs and SLB. The combination of the two techniques allowed highlighting even the smallest change in the SLB structure upon incubation with the NPs. In fact, while QCM-D gives information about the "wet mass" adsorbed (hydration water included) in terms of amount and viscoelastic properties of the surface layer, NR provides a structural characterization of the membrane in terms of thickness, roughness, hydration and selective composition of the tail and head regions of the membrane at a resolution able to quantify how these attributes are altered by the interaction with the nanomaterial.[33] The combination of the two techniques allowed highlighting even the smallest change in the SLB structure following the interaction with the NPs.

We present here a study performed with QCM-D,[6, 34-39] combined with NR[37, 40-43] aimed at exploring the effect of soft and hard protein coronas on the interaction of polystyrene (PS) NPs with supported lipid bilayers.

2. Experimental Section

2.1 Chemicals

1,2-Dioleoyl-sn-glycero-3-phosphocholine (DOPC) was obtained from Avanti Polar Lipids. Yellow-green carboxylate-modified polystyrene NPs were purchased from Invitrogen. Foetal bovine serum (FBS) was purchased from Fisher. Sucrose, sodium phosphate dibasic, potassium phosphate monobasic, sodium chloride and potassium chloride were from Sigma.

2.2 Preparation of supported lipid bilayer (SLB)

20 mg of DOPC were weighed and suspended in 1 ml of chloroform; the solvent was quickly evaporated with a rotary evaporator and left to dry under vacuum overnight. The dry film was hydrated with 1 ml of PBS at pH 7.4 and stirred to form a homogeneous suspension. Five cycles of freeze and thaw were performed and then the dispersion was extruded twice through 200 nm and 100 nm pore diameter membranes to obtain a monodisperse small unilamellar vesicle (SUV) dispersion. The SLB was formed applying a 0.5 mg/ml DOPC SUV dispersion in PBS at 37°C on silicon dioxide functionalized surface and deposition was optimised by QCM-D experiments[44]. Vesicles adhere to the surface and start to fuse forming a bilayer after a critical concentration of vesicles on the supporting surface is reached (see Figure 1).

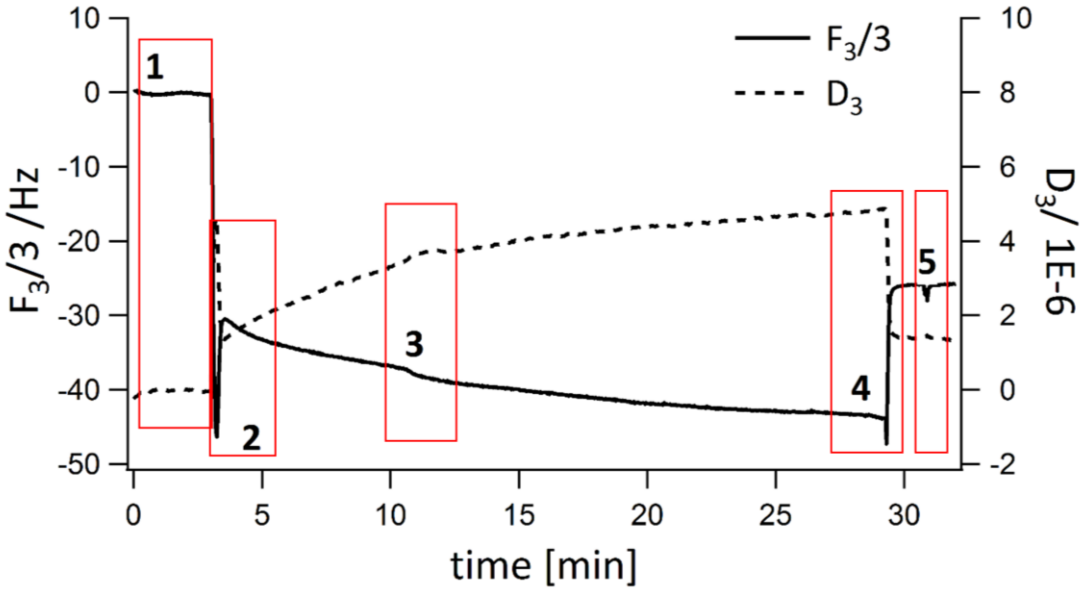

Figure 1. The frequency (solid line) and the dissipation (dashed line) profiles at the third overtone of DOPC SLB. The numbers and the squares in the figure indicate the different steps of formation of the SLB: 1) vesicles are injected in the chamber; 2) vesicles start forming the bilayer; 3) SLB is formed; 4-5) buffer washings are performed for removing excess of vesicles and obtaining a stable SLB.

2.3 Preparation of NP samples

Carboxylated polystyrene NPs with nominal diameter of 20 and 100 nm (provided by the manufacturer), named PS-COOH20 and PS-COOH100, were used. NPs were studied in several experimental conditions: a) in PBS; b) in 55% FBS dispersion after incubation at 37°C for 1 hour (*in situ*); c) as hard corona (HC) NPs isolated as previously described.[45] Briefly, isolation consists

of incubation of the NPs in 55% FBS (for 1h, at 37°C) and further purification from the excess of proteins by ultracentrifugation in sucrose gradient. The sucrose gradient layer in the range 4-40% w/w and the NPs were centrifuged for 120 min at 20°C at 110k RCF with a Beckman Coulter equipped by a SW41 Ti rotor. NPs, localized at a sucrose concentration of approximately 28% w/w, were recovered and dialyzed against PBS overnight at 4°C to remove the sucrose. The obtained HC NPs were characterized by DLS and Z-potential. Physical characterization of all used NPs in this study is reported in Table 1. While QCM-D experiments were performed with both NPs, Neutron Reflectometry experiments were only done with PS-COOH20 NPs (Table 1). NP concentration was chosen in order to operate in excess of NPs and saturate the surface of the quartz sensor (diameter of 14 mm): the QCM-D experiments were performed at concentrations relative to a total available surface area of 0.5-0.02 m^2/ml. For the NR experiments the NP concentration corresponded to a total surface area of 0.07 m^2/ml. Both QCM-D and NR experiments were performed on SLBs first treated with two injections of NP dispersions (to reach saturation) and then extensively washed with PBS.

Table 1. List of the NPs used in QCM-D and NR experiments. The NPs were characterized by size (d_H), polydispersivity index (PdI) and Z-potential (Zp) in different conditions: dispersed in PBS (*), dispersed in 55% v/v FBS PBS solution (*in situ*) and as hard corona (HC) NPs. The procedure to obtain the HC is described in the text.

	QCMD			NR		
	d_H [nm]	PdI	Zp [mV]	d_H[1] [nm]	PdI[2]	Zp [mV]
PS-COOH20*	32.3±0.4	0.10	-42±1	36.4±0.5	0.21	-38±3
PS-COOH100*	100.2±0.7	0.04	-34±1			
PS-COOH20 *in situ*	67.6±0.7	0.18	---	60.8±2.1	0.21	---
PS-COOH100 *in situ*	139.0±0.4	0.02	---			
PS-COOH20 HC	69.2±1.5	0.11	-9 ±2	83.6±0.9	0.16	-8±1
PS-COOH100 HC	173.0±2.9	0.20	-10±2			

2.4 QCM-D

The measurements were performed using a D300 - (Q-Sense AB, Västra Frölunda, Sweden) with a QAFC 302 axial flow measurement chamber maintained at 37 °C. QSX 303 silicon

dioxide sensors (Q-Sense AB, Västra Frölunda, Sweden) were used as the substrate. The sensor was excited, applying an alternating current across the sensor electrodes, at its fundamental resonant frequency (i.e. 5 MHz), and at the 3rd, 5th and 7th overtones. A sample volume of 0.7 ml was injected into the chamber containing the sensor crystal (internal volume, 50 µl) to ensure a complete solution exchange. QCM-D measures the frequency change (Δf) and the dissipation change (ΔD), at each of the four frequencies upon adsorption of matter onto the sensor surface. Changes in the frequency of the oscillating sensor were related to the changes in the hydrated mass adsorbing on to the quartz crystal sensor using the Sauerbrey model.[46]

$$\Delta m = - (\rho_q l_q / f_0) (\Delta f / n)$$

Δm is the hydrated mass (ng/cm^2), ρ_q (kg/m^3) and l_q (m) are respectively density and thickness of the crystal summarized in a constant of value 17.7 ng cm^{-2} Hz^{-1} at the fundamental frequency of 5 MHz.

Changes in dissipation were measured to determine the SLB viscoelasticity changes; as the dissipation (D) is inversely proportional to the decay time (τ) and resonant frequency (f) of the oscillating sensor as follows:

$$\Delta D = 1/\pi f \tau$$

ΔD is measured from the frequency exponential decay when the circuit is open. The softer the adsorbed layer, the faster the sensor stops oscillating (reducing decay time), and thus increasing dissipation. Data were analyzed by QTools software (Q-Sense AB, Västra Frölunda, Sweden). Before each experiment, the sensor was cleaned with 2% w/w SDS, rinsed in MQW, treated for 20 minutes in dilute nitric acid, rinsed with MQW, dried under nitrogen flow and finally exposed to UV light from a UV-Ozone chamber (BioForce Nanosciences, Inc., Iowa, USA) for minimum 15 min. All the experiments were conducted in triplicate. The solutions were kept at 37°C.

A representative QCM-D experimental profile of the SLB formation, frequency shift versus time, is described in Fig. 1. At time 1 the DOPC liposome dispersion is injected in the QCM-D chamber with a decrease of frequency (increase of dissipation). The vesicles start adhering on the silicon dioxide surface (time 2) and, as a critical concentration on the chip surface is reached, the vesicles start forming the bilayer and releasing water (increase of frequency, decrease of dissipation). At times 3 and 4 buffer is injected for removing the intact vesicles either adsorbed to the bilayer or free in solution, thus forming a stable bilayer (time 5). After the stable SLB has been formed, a first solution of NPs is injected. After equilibrium has been reached, another

solution of NPs is injected to ensure SLB saturation with NPs. Again, after the equilibrium has been achieved two successive PBS washings are performed.

2.5 Neutron Reflectometry (NR)

Specular reflectometry experiments were performed at the Institut Laue-Langevin (Grenoble, France) using the high flux D17 reflectometer.[47] Experiments were performed in time-of-flight mode, with a beam of wavelengths in the range 2-20 Å and at two angles of incidence (θ = 0.8° and 3°). D17 has a horizontal scattering geometry used to probe vertical surfaces. A flow cell with a chamber of dimensions ~7.5x4.5x0.1 cm^3 was used and the surface was silicon oxide. The solid substrates, (111) silicon single crystals of dimensions 8x5x1.5 cm^3, were cleaned by piranha solution (H_2SO_4: H_2O_2 3:1) for 20 minutes at 85°C and then they were washed extensively by MQW before assembling the cells and filling them with PBS buffer prepared with D_2O. Cells were kept at 37°C. Experiments were performed in different contrast conditions. 100% D_2O, 64% D_2O (four- matching water, 4MW), 38% D_2O (silicon- matching water, SMW), 100% H_2O.

In a neutron reflectivity experiment, reflectivity (R), the ratio between the intensities of the reflected and incident beams, is measured as a function of Q_z, the momentum transfer perpendicular to the interface.[48] In specular reflection, the detector is set to measure the neutrons scattered at an angle equal to that of the incident neutrons. In these conditions, Q vector is perpendicular to the surface and NR probes the scattering density (SLD) profile along this direction. The SLD is simply related to the composition of the interface and can be expressed as:

where n_j is the number of nuclei per unit volume, and b_j is the scattering length of nucleus j.

The model used to interpret experimental data can be described by a series of parallel layers of homogeneous material. Each layer is characterized by an average SLD, a thickness (t), a solvent penetration degree (φ) and a roughness (σ), which is treated as an error function. These parameters are used to calculate a model reflectivity profile by means of the optical matrix method. The quality of the fit is assessed comparing the experimental and calculated profiles by using χ^2 in the least-squares method. The model parameters are then adjusted to minimize χ^2.

Data were analyzed using Motofit, as previously described[33] allowing simultaneous fitting of data sets from the same sample under different contrast conditions. Two operating approaches were applied: 1) each block in the system is considered independent of the adjacent ("Rfit"); 2)

the model is reparametrized using physically relevant parameters to reduce the covariance of some parameters ("Gfit"). Each lipid layer was described in terms of a thickness (t_x), volume (V_x), and scattering length (b_x) of the tail and headgroup regions, their roughness, and area per molecule, APM. The SLDs for the head and tail layers are given by the ratio b/V. The volume fractions for the fragments are given by the ratio $V_{h,t}$ / $\mathrm{At}_{\mathrm{h,t}}$. The volume occupied by water is 1-V/At. The SLD for the layer is then:

$$SLD_{h,t} = (V_{h,t}/\mathrm{At}_{\mathrm{h,t}}) \times (b_{h,t}/(\mathrm{At}_{h,t}) + b_{solv}\,(1-V_{h,t}/\mathrm{At}_{\mathrm{h,t}})$$

The only parameters that vary during the fit are the area per molecule, common to the two fragments of the lipid, the thickness and the roughness. The other values can be found in literature[49] and are reported in Table 2.

To test the presence of adsorbed proteins, a 6th layer was added to the model (see Fig. S1) in some cases. Since the main component of the FBS is the bovine serum albumin (BSA), we assigned to this layer a thickness in the range of 50-70 Å[50] compatible with the BSA. The SLD was calculated for the different solvent isotopic compositions (*http://psldc.isis.rl.ac.uk/Psldc/*) based on the amino-acid sequence Q56G89 (UniProt).

Table 2. Structural parameters describing headgroup and tail fragments in DOPC lipid bilayer reported in Nagle et al.[49]

		DOPC
V_t [Å^3]	Tail volume	984

V_L [Å^3]	Lipid molecular volume	1303
APM [Å^2]	Area per molecule	72.5
D_c [Å]	Thickness of the hydrocarbon core	13.5
D_h [Å]	Headgroup thickness	9
b_h^* [Å]	Headgroup scattering length	$6x10^{-4}$
b_t^* [Å]	Tail scattering length	$-2.1x10^{-4}$
SLD_h^{**} [Å^{-2}]	Head scattering length density	$1.88x10^{-6}$
SLD_t^{**} [Å^{-2}]	Tail scattering length density	$-0.21x10^{-6}$

* Calculated by *http://sld-calculator.appspot.com/*; ** calculated by the ratio b/V.

3. Results

3.1 Rationale of the experimental protocol

The interaction of carboxylated polystyrene NPs with SLB was studied by means of QCM-D and NR experiments. In particular, we analyzed the structural changes of the SLB upon exposure to 20 nm carboxylated PS (PS-COOH20) NP dispersions in different conditions:

(i) in phosphate buffer solution (PBS, bare NPs),

(ii) in 55% (w/V) fetal bovine serum (FBS) (*in situ*)

(iii) isolated as hard corona NPs (HC) from FBS following the protocol explained above.[45]

The experimental protocol used to study the SLB morphology (thickness, coverage and viscoelasticity) after treatment with the NP dispersions consisted of 5 different steps: 1) assessment of the formation of a stable bilayer, 2) assessment of the structural properties of the SLB after treatment with a dispersion of NPs, 3) assessment of the structural properties of the SLB after a new injection of the same NP dispersion at the same concentration, 4) assessment of the structural properties of the SLB after a first wash with PBS, 5) final assessment of the structural properties of the SLB after a second wash with PBS. The last two steps were used to determine the final state of the lipid bilayer after extensive washing.

Before the formation of the SLB, the DOPC liposomal dispersion was characterized in terms of size and surface charge by DLS and Zeta potential (Fig. S2 and Table S1). The assessment of the formation of a stable SLB was done by QCM-D (Table S2) and NR. The scattering curves

obtained from the pristine SLB at the D_2O contrast are shown in Fig. S3 in the ESI and the complete list of the structural results obtained for the pristine SLBs are listed in Table S3.

3.2 NP-SLB interaction in phospate-buffered saline (PBS)

QCM-D and NR experiments were done before and after incubating the DOPC SLB with PS-COOH20 NPs dispersed in PBS following the protocol detailed above. In Figure 2 we display the equilibrium asymptotic values of the frequency shift, Δf, and dissipations, ΔD, measured after each phase of the experimental protocol. While exposure to a dispersion of NPs did not cause major immediate changes of Δf and ΔD, after washings with buffer, Δf shifted to less negative values and ΔD increased. In particular, a slight initial increase of ΔD in the presence of the NPs was followed by a more pronounced decrease upon buffer washing. This behavior was invariant with NP concentration (0.02 m^2/ml - 0.5 m^2/ml, Fig. S4a). Increasing the size of the NPs from 20 to 100 nm, instead, produced a relevant change in the observed trend: the frequency shifted toward more negative values and the dissipation increased significantly, as it can be seen in Fig. S4b-c in the ESI.

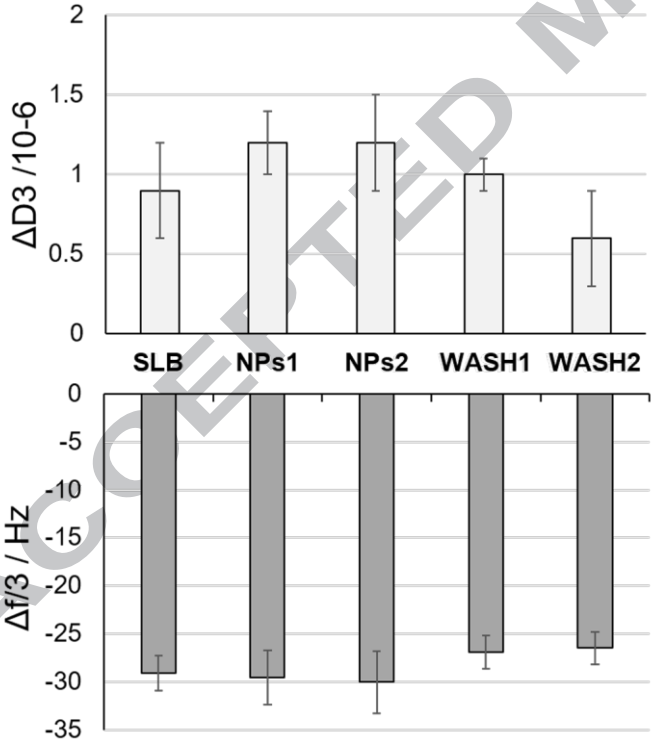

Figure 2. The effect of NPs on the SLB in terms of shift in frequency, Δf, and dissipation, (ΔD), obtained from QCM-D experiments of bare SLBs and SLBs treated with PS-COOH20 NPs in

PBS. We report the equilibrium values of the Δf at the third overtone, Δf/3, and the correspondent changes in dissipation, ΔD3 for each step of QCM-D experimental protocol.

Neutron reflectivity profiles of DOPC SLB before and after the exposure to the NP dispersions at different contrasts are displayed in Fig. 3a and b, respectively, where solid lines are the best fits to the experimental data based on the five slabs model described in the Experimental Section. The SLB on the Si surface was modelled as a 5 layers system that includes an oxide layer, the heads and the tails of the inner phospholipid leaflet in contact with the substrate, the tails and the heads of the outer leaflet in contact with the medium. A comparison between the NR profiles of the SLB before and after exposure to the NPs at a 38% D_2O contrast is shown in Fig. S5 in the ESI. Qualitatively, the curves of treated and untreated SLBs exhibit a similar trend with slight differences in the value of the maximum and a shift of the minimum in the high momentum transfer, Q, region. The parameters from the model that best fit the data are summarized in Table 3 (for the complete set refer to Table S3 in the ESI) and the effect of the interaction with the NP can be visually interpreted by looking at the scattering length density profiles (SLDs) derived by the analysis (Fig. 3c). The main effects on the SLD are due to hydration of the tail and head regions. The area per molecule (APM) of the leaflets increases from 72.0 ± 0.6 $Å^2$ up to 75.0± 2.0 $Å^2$. The increment in the hydration can be visualised as a spread in the SLD profiles in the tail region caused by the presence of the hydration water with different isotopic composition.

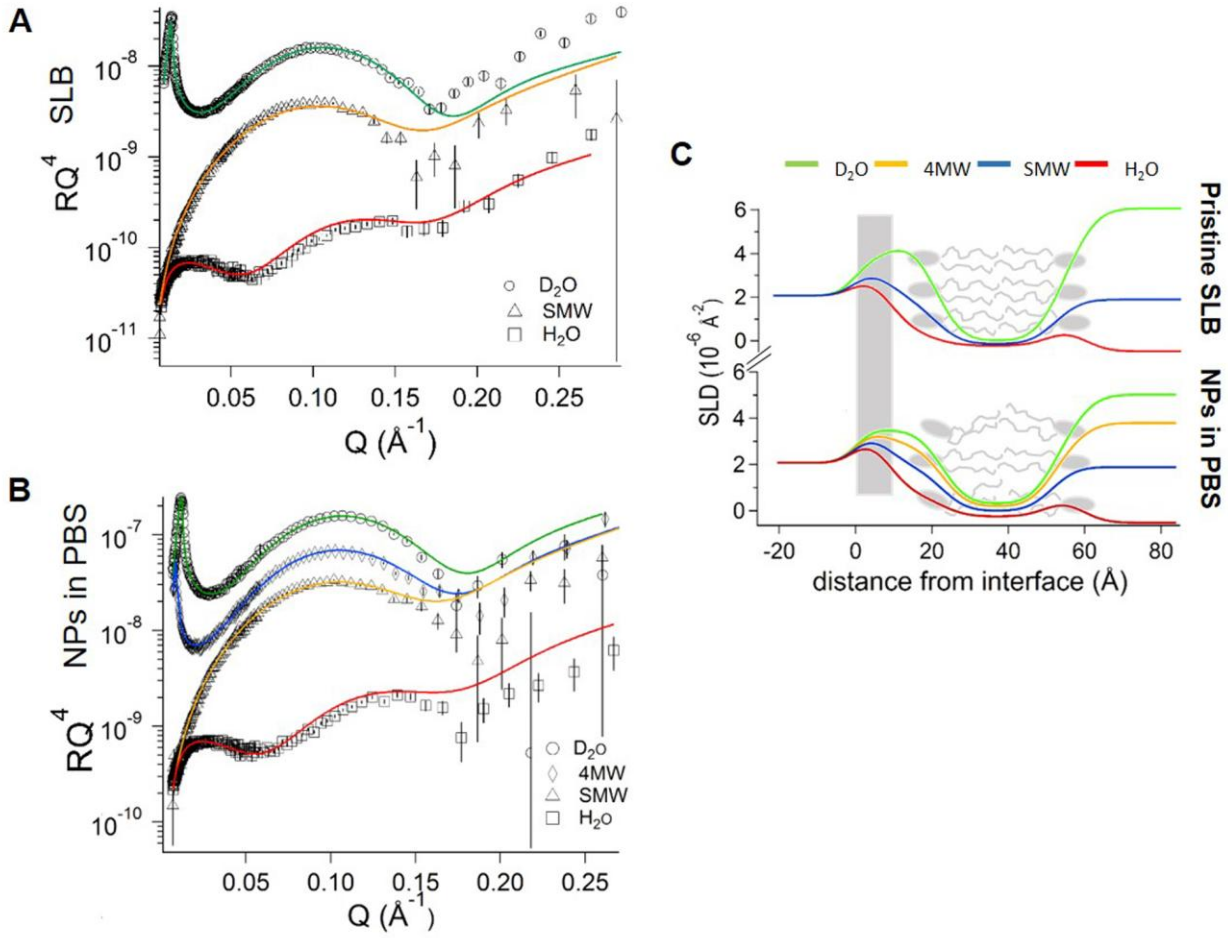

Figure 3. Structural effects on the SLB after exposure to PS-COOH20 NPs in PBS observed in NR experiments. A-B) NR data (symbols) and fitting curves (lines) before (A) and after (B) injection of the NPs. The fitting curves were obtained by simultaneous co-refinement of the NR curves measured at three or four contrasts (D_2O, 4MW, SMW, H_2O) to the 5-slab model described in the text. C) SLD profiles obtained by the co-refinement before (top) and after (bottom) the exposure to NPs.

Table 3. Structural details of the SLB obtained by the fitting analysis based on a five layers model before and after exposure to the PS-COOH20 NPs in PBS (from data showed in Figure 3).

Layer	t [Å]*		Φ*	
	SLB	SLB+NP	SLB	SLB+NP

Inner head	12.0±0.5	11.8±0.5	62±2	64±2
Inner tail	14.0±0.5	14.5±0.5	**1.0±1.0**	**9±3**
Outer tail	14.0±0.5	14.5±0.5	**1.0±1.0**	**9±3**
Outer head	6±1	6±1	**22±14**	**29±15**

*Model with constrains was applied. The parameters describing the SiO_2 layer and the roughness of the layers were kept constant to evaluate the effects on thicknesses (t) and solvent penetration (φ).

3.2 NP-SLB *in situ* interaction in 55% FBS

In the second set of experiments we analysed the protein effect on the structure of the SLB dispersing PS-COOH20 NPs in a 55% FBS solution (*in situ* NPs). When the NPs are in contact with the FBS both hard and soft protein coronas are adsorbed on their surface, which modulate the interaction with the SLB. To disentangle the effect due to free proteins and NP-associated proteins, we also performed a control measurement in the presence of FBS without NPs.

The QCM-D data obtained for SLBs treated with 55% FBS and *in situ* NPs dispersed in 55% FBS at the various stages of the protocol are shown in Fig. 4. In the presence of *in situ* NPs, we observed a shift of the frequency toward more negative values and an increase of the dissipation that persisted after washing. Instead, treating the SLB with 55% FBS medium the same initial changes were restored to the initial value after washing.

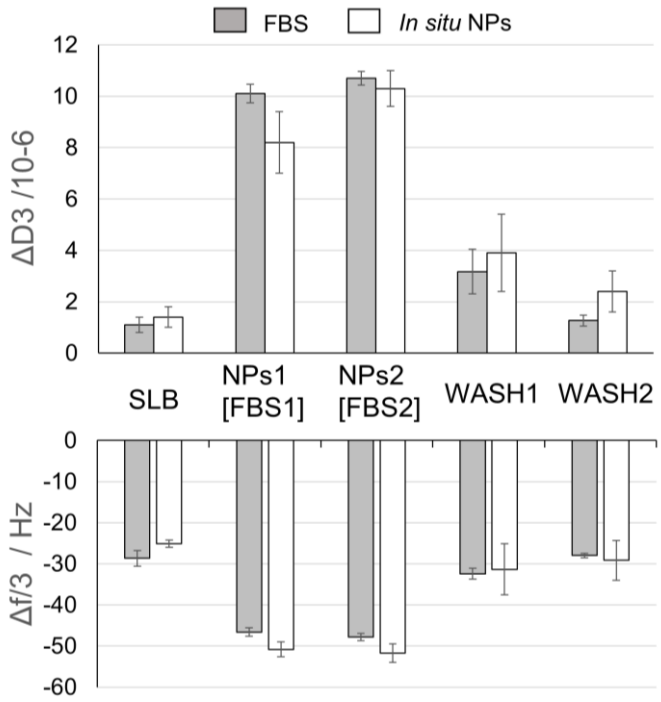

Figure 4 Effect of NP on the SLB in terms of shift in frequency, Δf, and dissipation, (ΔD), obtained from QCM-D experiments of bare SLBs and SLBs treated with PS-COOH20 NPs 55% FBS. We report the equilibrium values of the Δf at the third overtone, Δf/3, and the correspondent changes in dissipation, ΔD3 for each step of QCM-D experimental protocol.

The NR profiles for analogue SLB samples treated with *in situ* NPs and pure FBS solutions are displayed in Fig. 5. A direct comparison between the two cases showed a decrease of intensity of the fringe at 0.1 $Å^{-1}$ with respect to the pattern of the untreated SLB for both samples, the effect was enhanced in the presence of the NPs (Fig. 5b). A summary of the parameters and the scattering length density profiles obtained by fitting the data with the five slabs model can be found in Table 4 and in Fig. 5c, respectively. The presence of the NPs led to a significant increase of the hydration of the lipid bilayer mostly in the tail region together with a small swelling of such a region as shown by the values reported in Table 4. On the contrary, FBS alone did not significantly affect the SLB. Given the high concentration of proteins in the environment, we also tried to model the reflectivity profiles with an additional sixth layer of proteins (Fig. S6a-b and Table S4 in the ESI). Adding a sixth layer of protein did nor result in an improvement in the χ^2 (see Tables S3 and S4) and the hypothesis was dismissed.

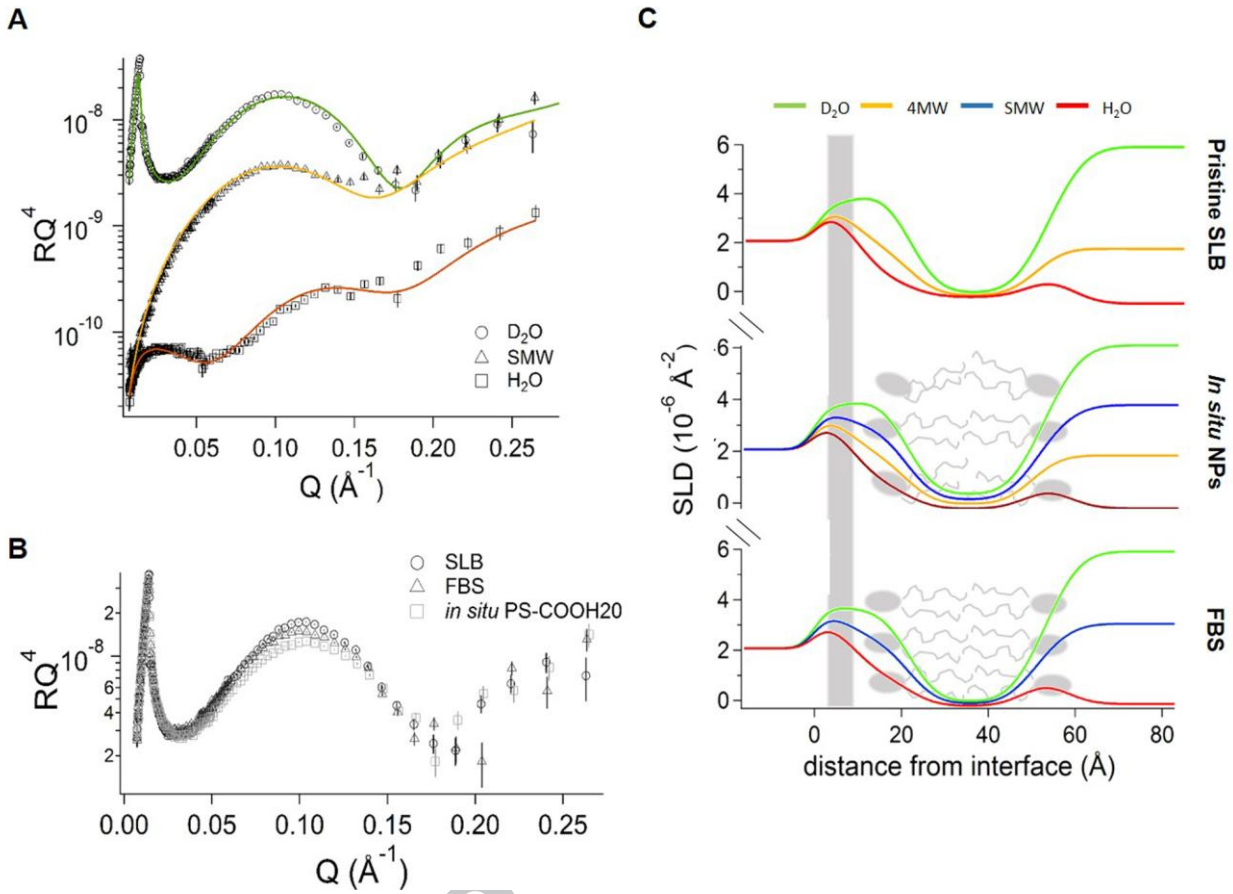

Figure 5. The structural effects on the SLB after exposure to *in situ* PS-COOH20 NPs and 55% FBS solutions observed by NR experiments. A) NR data (symbols) of the pristine SLB and fitting curves (lines) obtained by simultaneous co-refinement of the NR curves at three contrasts (D_2O, SMW, H_2O) to the 5-slab model described in the text. B) NR data (symbols) of the pristine SLB, after treatment with a solution of 55% FBS and after treatment with *in situ* NPs (see legend). C) SLD profile of the pristine SLB (top), of the SLB treated with *in situ* NP (middle) and of the SLB treated with 55% FBS (bottom).

Table 4. NR results from the 5-slab fitting of the SLB prior and after exposure to the PS-COOH20 NPs in 55% FBS.

	t [Å]*			Φ*		
Layer	SLB	FBS	NPs	SLB	FBS	NPs
Inner head	11.0±0.5	11.0±0.5	11.0±0.5	60±2	59±2	60±3
Inner tail	14.0±0.5	14.0±0.5	**15.0±0.5**	2±2	**3±3**	**11±4**
Outer tail	14.0±0.5	14.0±0.5	**15.0±0.5**	2±2	**3±3**	**11±4**
Outer head	6±1	6±1	**7±1**	27±18	**28±15**	**36±15**

*Model with constrains was applied. The parameters describing the SiO_2 layer and the roughness of the layers were kept constant to evaluate the effects on thicknesses (t) and solvent penetration degrees (φ).

3.3 NP-SLB interaction in the presence of hard-corona (HC) NPs

The last series of experiments aimed to determine the effect of HC NPs isolated from 55% FBS (i.e. without excess of free proteins) on the structure of the lipid bilayer. QCM-D experiments performed applying HC NPs to the SLB resulted in minor changes: a slight shift in the frequency towards values that are more negative and a small increase in the dissipations (Fig. 6). The NR data reported in Fig. 7 and Table 5 are in agreement with what found by QCM-D, the SLB structure was almost unaffected by treatment with HC NP dispersion at the same NP concentration used in the previous experiments.

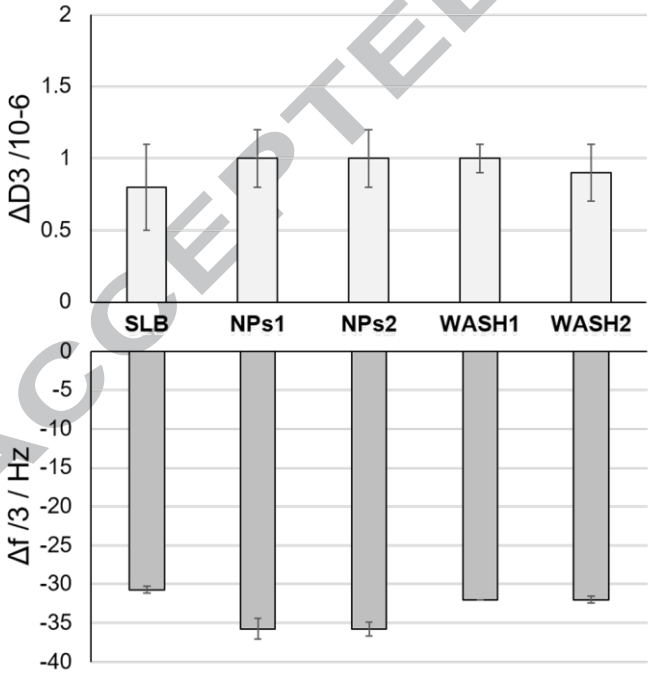

Figure 6. The effect of the NPs on the SLB in terms of shift in frequency, Δf, and dissipation, ΔD, obtained from QCM-D experiments on SLB treated with PS-COOH20 HC NPs. We report the equilibrium values of the Δf at the third overtone, Δf/3, and the corresponding changes in dissipation, ΔD3 for each step of QCM-D experimental protocol.

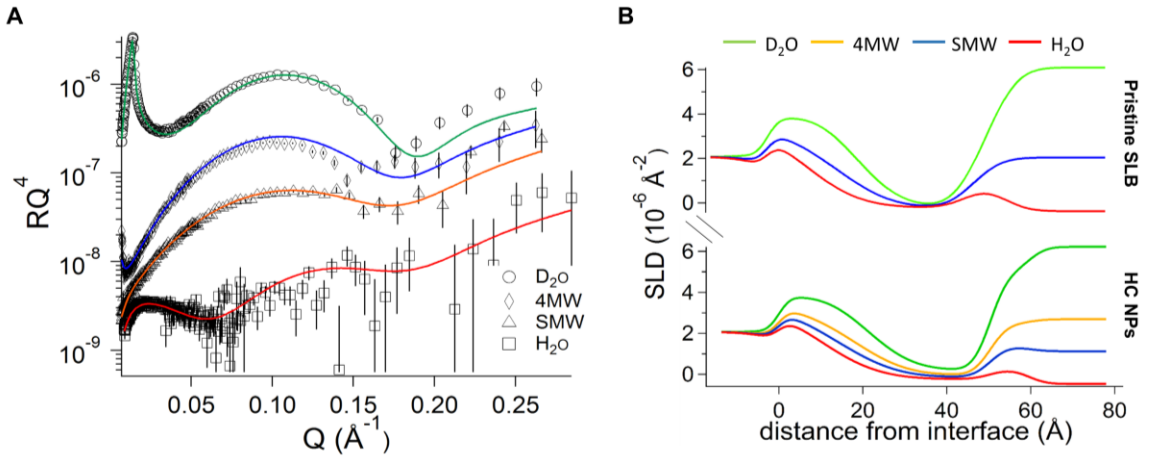

Figure 7. Structural effects on the SLB after exposure to HC PS-COOH20 NPs: A) NR data (symbols) and fitting curve (D_2O, 4MW, SMW, H_2O) of the SLB after treatment with HC PS-COOH20 NPs; B) SLD profile of the pristine SLB (top) and after HC NP treatment (bottom).

Table 5. Results from the 5-slab fitting of the NR data from the SLB prior and after exposure to HC PS-COOH20 NPs.

Layer	t [Å]*		Φ*	
	SLB	NPs	SLB	NPs
Inner head	12.0±0.5	12.0±0.5	62±1	63.0±0.5
Inner tail	14.0±0.5	14.0±0.5	1±1	1±1

Outer tail	14.0±0.5	14.0±0.5	1±1	1±1
Outer head	6±1	6±1	23±14	19±14

*Model with constrains was applied. The parameters describing the SiO_2 layer and the roughness of the layers were kept constant to evaluate the effects on thicknesses (t) and solvent penetration degrees (φ).

4. Discussion

The SLBs used in QCM-D and NR experiments were formed from a dispersion of lipid vesicles by spontaneous adsorption and re-arrangement of the deposited vesicles on SiO_2 surfaces. The resulting SLBs were extensively washed with buffer for eliminating excess of vesicles and showed to be extremely stable and reproducible in both QCM-D and NR experiments. Thickness and viscoelasticity values obtained by QCM-D are in agreement with those reported in the literature,[44] with a frequency shift of about -25 Hz and a dissipation below 2. The hydration mass includes the coupled water that is the solvent layer between the sensor and the lipid bilayer and it was estimated to have a value of about 102 ng/cm.[13, 51]

The NR characterisation of DOPC SLB agrees with data reported in literature.[49, 52-54] Curves are characterized by a minimum between 0.15 and 0.20 $Å^{-1}$ related to the thickness of the bilayer, due to interference arising between the reflected waves at the top and the bottom of the SLB. The defects in the SLB can be evaluated from the amount of hydration water in the hydrophobic tails region of the SLB. The averaged value of tail hydration was less than 1% (0.8±0.3%) indicating essentially defect free layers.

The thickness value of SLBs determined with the two techniques is the same (46 ± 6 Å and 46 ± 5 Å, respectively). NR allows higher molecular resolution to distinguish between hydrophilic and hydrophobic regions: the hydrophobic tail region was 28.3 ± 0.6 Å, slightly larger than that provided by Nagle *et al.*[49] (27.1 Å at 30°C), the outer polar head region had a thickness equal to about one half of the inner one. This asymmetry of the profiles can be due to the different distribution of hydration water and the thermal motions that affect the thickness of the head regions at the interfaces.[53-55] Moreover, the two lipid leaflets, the inner (L2-3) and the outer (L4-5) experienced different environments, as the inner leaflet was in direct contact with the SiO_2 layer and water confined between the solid surface and the headgroup layer is expected (L1).[41]

The pre-formed SLB was then treated with the NPs dispersed in different environments. First, the dependence of the NP concentration was studied in terms of changes in the SLB (Fig. S3a). QCM-D results showed that the SLB was not disrupted by treatment with any concentration of

PS-COOH20 NPs (unchanged dissipation showed in Fig. 2). The trend for all concentrations was similar: initially a small amount of PS-COOH20 NPs adsorbed on the SLB, which were removed by washing with additional loss of mass with respect to the initial value. The decrease in hydrated mass of the bilayer was about 50 ng, roughly 10% of the initial adsorbed mass. This mass loss can be interpreted in two ways: either due to membrane shrinkage with loss of water upon NPs adsorption onto the SLB or to lipid adsorption on the NP surface with a consequent lipid loss from the SLB. NR experiments allowed the detection of molecular changes on the structure of the SLB indicating lipid extraction upon NP interaction. In fact, the results reported in Table 2 and Table S3 in the ESI show a change in DOPC APM from an initial value of 72.0 ± 0.6 $Å^2$, in agreement with the literature[53], up to 75.0± 2.0 $Å^2$ after NP treatment. This change was interpreted as decrease of lipid packing, inversely proportional to the APM, due to a loss of lipids induced by desorption of the anionic NPs upon washing. This hypothesis was also supported by an increased hydration of the hydrophobic tail region. Other studies on the effect of carboxylated NPs on lipid bilayers highlighted different effects: Negoda and co-workers reported the formation of pores in DOPC bilayers formed on a Delrin cup upon exposure to carboxylated NPs.[56] We speculate that a SLB (as in our case) is more resistant to external stimulus and no pores are formed. Anionic PS NPs of the same size but different surface charge density were found to adsorb on DOPC LUVs (large unilamellar vesicles) inducing a local fluid to gel transition of the lipids with consequent shrinking of the membrane, decrease of the APM and loss of hydration due to NP binding.[7] The different behaviour is ascribed to a different NP surface charge density and the system geometry (SLB versus LUV) making difficult a direct comparison.

To evaluate the effect of the NP size we performed the same experiments using 100 nm carboxylated polystyrene NPs, keeping constant the total NP surface available (see Fig. S4b-c). Interestingly, PS-COOH100 NPs, unlike PS-COOH20 NPs, caused a significant decrease of frequency and increase of dissipation. The increase in dissipation indicates that PS-COOH100 NPs were adsorbed on the SLB and/or on the SiO_2 surface causing major lipid removal with consequent breakage of the lipid bilayer. Since the Z-potential and the surface chemistry of the NPs are similar, as well as the total exposed surface area in the chosen experimental conditions, the major destabilization of the SLB structure was ascribed to the NP size.

After having studied the NP effect on the SLB in buffer, we investigated how the presence of proteins in the environment could alter the NP-SLB interaction in relation to the different role of hard and soft coronas.

We isolated HC NPs and re-suspended them in PBS. HC NPs showed a very low tendency to bind to the SLB even in saturation conditions (Fig. 6) and did not show any significant effect on the viscoelastic properties of the SLB indicating a weak interaction. The lower tendency of HC NPs to adsorb and/or interact with the SLB was more evident with PS-COOH100 NPs, where the effect was more remarkable considering that the same NPs dispersed in PBS induced the rupture of the SLB. The HC composition of the differently sized NPs was different as shown in Fig. S7 in the ESI, but in both cases the presence of a HC strongly reduced the interaction with the SLB. NR experiments confirmed the trend highlighted by QCM-D results, indicating that the HC completely hampers the non-specific interaction between NPs and SLB. Thus, it seems that the NP-SLB interaction is mainly driven by the high surface energy of the bare NPs that tend to extract lipids from the bilayer.[16,57] Montis and co-workers[58] observed a mild structural reorganization of giant unilamellar vesicles (GUV) lipid bilayers composed of POPC (1-palmitoyl-2-oleoyl-sn-glycero-3-phosphocholine) induced by HC citrate capped 15 nm Au NPs, indicating an important role of both lipid composition and NP features. The NPs were incubated with 10% FBS and the excess of proteins removed by centrifugation.

Although the HC constitutes the most permanent protein shell on the NP surface and it is considered the biological identity of the NP, a soft corona is also associated *in vivo* to the NPs and its role in the bio-nano-interaction is still elusive. For this reason, experiments with pure serum and NPs in serum were performed, to investigate if weakly associated and free proteins have a role in the NP-SLB interaction. The QCM-D experiments revealed a certain amount of mass adsorbed on the SLB after extensive washings for both samples (Fig. 4). Comparing the NR profiles of the lipid bilayer in the presence of proteins, a decrease in intensity of the fringe at 0.1 $Å^{-1}$ could be observed, and the effect was enhanced in the presence of the NPs. Le Brun and co-workers observed a similar effect in the presence of only proteins.[59] They studied the interactions of some fragments of prion proteins with zwitterionic and anionic SLBs. They did not see any interaction with the neutral SLB, while they found a highly solvated layer of peptide (0.15 volume fraction) adsorbed on the anionic SLB. They performed a deep analysis on the structural SLB reorganization upon peptides interaction, which unluckily was not applicable in our case for the heterogeneity of the medium composed of proteins with different sizes and

charges. FBS-induced destabilization of SLBs was also reported by Peetla *et al.*[10] who observed a small decrease of surface pressure of DPPC SLBs upon treatment with 10% FBS. The decrease of surface pressure was interpreted as a sign of lipid condensation and was attributed to either protein embedding in the SLB with subsequent reduction of the APM of the lipids or electrostatic interactions between proteins and polar heads with decrease of the repulsive forces between lipids inducing compression.

In our case, pure FBS induced minor changes in the SLB structure. On the other hand, swelling and a significant increase of the hydration were observed in the presence of the NPs as consequence of lipid interaction with the soft protein corona.

Notwithstanding the limitation of our model with respect to a cellular membrane for which the structure is much more complex, we can state that both shear flow[60] and excess of proteins, which reduce NP surface free energy,[23,61] influence NP adhesion to lipid membranes when unspecific interactions are predominant. Overall, our results suggest that while the presence of hard corona flattens the interaction between NPs and model lipid bilayers, the associated soft corona affects the structure of the bilayer in a different way compared to free proteins.

5. Conclusions

In this work we investigated the interaction of NPs with model lipid membranes. DOPC SLBs were used as simple models to mimic a biological membrane and in-flow experiments were performed to study the effect of NPs on the lipid bilayer structure. The role of proteins, either free in the environment or included in the hard and soft coronas was explored. The study was based on the coupling of QCM-D and NR techniques. The changes detected in the acoustic resonator of the QCM-D were related to quantitative changes in the nanostructure of the SLB as measured by the NR technique.

This study contributes to enrich the knowledge on NP-membrane interaction in the presence of proteins adding a new tile to this puzzle. The size (and curvature) of the investigated NPs showed an important role in their interaction with the SLB. We also found that soft corona NPs, so far not considered important for such interactions, induced permanent alteration in the lipid bilayer structure contrarily to free serum, while we confirmed that hard corona NPs weakly interact with SLBs compared to their bare counterparts. The next step would be elaborating membrane models closer to cell membranes (for example by including in the SLB formulation cholesterol, membrane proteins, charges, etc.) and investigating further the role of soft corona in

cell-NPs interactions, which has not been deeply studied so far due to the difficulties of isolating these complexes and defining their exact composition.

Acknowledgements

We acknowledge the Institut Laue-Langevin for beam time allocation and the Partnership for Soft Condensed Matter (PSCM) for the use of their laboratories. This work was supported by funds from the British Skin Foundation and the Royal Society.

Supporting Information. In the electronic supporting information (ESI_disilvio.pdf)

REFERENCES

1. Mahmoudi, M.; Meng, J.; Xue, X.; Liang, X. J.; Rahman, M.; Pfeiffer, C.; Hartmann, R.; Gil, P. R.; Pelaz, B.; Parak, W. J.; Del Pino, P.; Carregal-Romero, S.; Kanaras, A. G.; Tamil Selvan, S., Interaction of stable colloidal nanoparticles with cellular membranes. *Biotechnology advances* **2014,** *32* (4), 679-692.
2. Rascol, E.; Devoisselle, J. M.; Chopineau, J., The relevance of membrane models to understand nanoparticles-cell membrane interactions. *Nanoscale* **2016,** *8* (9), 4780-4798.
3. Wu, L.; Jiang, X., Recent developments in methodology employed to study the interactions between nanomaterials and model lipid membranes. *Anal Bioanal Chem* **2016,** *408* (11), 2743-2758.
4. dos Santos, T.; Varela, J.; Lynch, I.; Salvati, A.; Dawson, K. A., Quantitative Assessment of the Comparative Nanoparticle-Uptake Efficiency of a Range of Cell Lines. *Small* **2011,** *7* (23), 3341-3349.
5. Cheng, L.-C.; Jiang, X.; Wang, J.; Chen, C.; Liu, R.-S., Nano-bio effects: interaction of nanomaterials with cells. *Nanoscale* **2013,** *5* (9), 3547-3569.
6. Jing, Y.; Trefna, H.; Persson, M.; Kasemo, B.; Svedhem, S., Formation of supported lipid bilayers on silica: relation to lipid phase transition temperature and liposome size. *Soft Matter* **2014,** *10* (1), 187-195.
7. Wang, B.; Zhang, L.; Bae, S. C.; Granick, S., Nanoparticle-induced surface reconstruction of phospholipid membranes. *Proceedings of the National Academy of Sciences* **2008,** *105* (47), 18171-18175.
8. Schulz, M.; Olubummo, A.; Binder, W. H., Beyond the lipid-bilayer: interaction of polymers and nanoparticles with membranes. *Soft Matter* **2012,** *8* (18), 4849-4864.
9. Ouberai, M. M.; Wang, J.; Swann, M. J.; Galvagnion, C.; Guilliams, T.; Dobson, C. M.; Welland, M. E., α-Synuclein Senses Lipid Packing Defects and Induces Lateral Expansion of Lipids Leading to Membrane Remodeling. *Journal of Biological Chemistry* **2013,** *288* (29), 20883-20895.
10. Peetla, C.; Labhasetwar, V., Biophysical Characterization of Nanoparticle−Endothelial Model Cell Membrane Interactions. *Molecular Pharmaceutics* **2008,** *5* (3), 418-429.

11. Chen, Y.; Bothun, G. D., Cationic Gel-Phase Liposomes with "Decorated" Anionic SPIO Nanoparticles: Morphology, Colloidal, and Bilayer Properties. *Langmuir* **2011,** *27* (14), 8645-8652.
12. Leroueil, P. R.; Berry, S. A.; Duthie, K.; Han, G.; Rotello, V. M.; McNerny, D. Q.; Baker, J. R.; Orr, B. G.; Banaszak Holl, M. M., Wide Varieties of Cationic Nanoparticles Induce Defects in Supported Lipid Bilayers. *Nano Letters* **2008,** *8* (2), 420-424.
13. Verma, A.; Stellacci, F., Effect of Surface Properties on Nanoparticle–Cell Interactions. *Small* **2010,** *6* (1), 12-21.
14. Shang, L.; Nienhaus, K.; Nienhaus, G. U., Engineered nanoparticles interacting with cells: size matters. *Journal of Nanobiotechnology* **2014,** *12* (1), 5.
15. Mhashal, A. R.; Roy, S., Effect of Gold Nanoparticle on Structure and Fluidity of Lipid Membrane. *PLoS ONE* **2014,** *9* (12), e114152.
16. Li, Y.; Chen, X.; Gu, N., Computational Investigation of Interaction between Nanoparticles and Membranes: Hydrophobic/Hydrophilic Effect. *The Journal of Physical Chemistry B* **2008,** *112* (51), 16647-16653.
17. Kim, S. T.; Saha, K.; Kim, C.; Rotello, V. M., The Role of Surface Functionality in Determining Nanoparticle Cytotoxicity. *Accounts of Chemical Research* **2013,** *46* (3), 681-691.
18. Jing, B.; Zhu, Y., Disruption of Supported Lipid Bilayers by Semihydrophobic Nanoparticles. *Journal of the American Chemical Society* **2011,** *133* (28), 10983-10989.
19. Pelaz, B.; del Pino, P.; Maffre, P.; Hartmann, R.; Gallego, M.; Rivera-Fernández, S.; de la Fuente, J. M.; Nienhaus, G. U.; Parak, W. J., Surface Functionalization of Nanoparticles with Polyethylene Glycol: Effects on Protein Adsorption and Cellular Uptake. *ACS Nano* **2015,** *9* (7), 6996-7008.
20. Rocha, E. L. d.; Caramori, G. F.; Rambo, C. R., Nanoparticle translocation through a lipid bilayer tuned by surface chemistry. *Physical Chemistry Chemical Physics* **2013,** *15* (7), 2282-2290.
21. Walczyk, D.; Bombelli, F. B.; Monopoli, M. P.; Lynch, I.; Dawson, K. A., What the Cell "Sees" in Bionanoscience. *Journal of the American Chemical Society* **2010,** *132* (16), 5761-5768.
22. Corbo, C.; Molinaro, R.; Tabatabaei, M.; Farokhzad, O. C.; Mahmoudi, M., Personalized protein corona on nanoparticles and its clinical implications. *Biomaterials Science* **2017,** *5* (3), 378-387.
23. Lesniak, A.; Salvati, A.; Santos-Martinez, M. J.; Radomski, M. W.; Dawson, K. A.; Åberg, C., Nanoparticle Adhesion to the Cell Membrane and Its Effect on Nanoparticle Uptake Efficiency. *Journal of the American Chemical Society* **2013,** *135* (4), 1438-1444.
24. Hirano, A.; Uda, K.; Maeda, Y.; Akasaka, T.; Shiraki, K., One-Dimensional Protein-Based Nanoparticles Induce Lipid Bilayer Disruption: Carbon Nanotube Conjugates and Amyloid Fibrils. *Langmuir* **2010,** *26* (22), 17256-17259.
25. Fleischer, C. C.; Payne, C. K., Secondary Structure of Corona Proteins Determines the Cell Surface Receptors Used by Nanoparticles. *The Journal of Physical Chemistry B* **2014,** *118* (49), 14017-14026.
26. Jiang, W.; Lai, K.; Wu, Y.; Gu, Z., Protein corona on magnetite nanoparticles and internalization of nanoparticle–protein complexes into healthy and cancer cells. *Arch. Pharm. Res.* **2014,** *37* (1), 129-141.
27. Di Silvio, D.; Rigby, N.; Bajka, B.; Mackie, A.; Baldelli Bombelli, F., Effect of protein corona magnetite nanoparticles derived from bread in vitro digestion on Caco-2 cells

morphology and uptake. *The international journal of biochemistry & cell biology* **2016,** *75*, 212-222.
28. Ritz, S.; Schöttler, S.; Kotman, N.; Baier, G.; Musyanovych, A.; Kuharev, J.; Landfester, K.; Schild, H.; Jahn, O.; Tenzer, S.; Mailänder, V., Protein Corona of Nanoparticles: Distinct Proteins Regulate the Cellular Uptake. *Biomacromolecules* **2015,** *16* (4), 1311-1321.
29. Mirshafiee, V.; Kim, R.; Park, S.; Mahmoudi, M.; Kraft, M. L., Impact of protein pre-coating on the protein corona composition and nanoparticle cellular uptake. *Biomaterials* **2016,** *75*, 295-304.
30. Cheng, X.; Tian, X.; Wu, A.; Li, J.; Tian, J.; Chong, Y.; Chai, Z.; Zhao, Y.; Chen, C.; Ge, C., Protein Corona Influences Cellular Uptake of Gold Nanoparticles by Phagocytic and Nonphagocytic Cells in a Size-Dependent Manner. *ACS Applied Materials & Interfaces* **2015,** *7* (37), 20568-20575.
31. Lesniak, A.; Fenaroli, F.; Monopoli, M. P.; Åberg, C.; Dawson, K. A.; Salvati, A., Effects of the Presence or Absence of a Protein Corona on Silica Nanoparticle Uptake and Impact on Cells. *ACS Nano* **2012,** *6* (7), 5845-5857.
32. Luchini, A.; Gerelli, Y.; Fragneto, G.; Nylander, T.; Palsson, G. K.; Appavou, M. S.; Paduano, L., Neutron Reflectometry reveals the interaction between functionalized SPIONs and the surface of lipid bilayers. *Colloids and surfaces. B, Biointerfaces* **2017,** *151*, 76-87.
33. Tatur, S.; Maccarini, M.; Barker, R.; Nelson, A.; Fragneto, G., Effect of functionalized gold nanoparticles on floating lipid bilayers. *Langmuir : the ACS journal of surfaces and colloids* **2013,** *29* (22), 6606-6614.
34. Choi, S. Y.; Jeong, S.; Jang, S. H.; Park, J.; Park, J. H.; Ock, K. S.; Lee, S. Y.; Joo, S.-W., In vitro toxicity of serum protein-adsorbed citrate-reduced gold nanoparticles in human lung adenocarcinoma cells. *Toxicology in Vitro* **2012,** *26* (2), 229-237.
35. Dabkowska, A. P.; Michanek, A.; Jaeger, L.; Rabe, M.; Chworos, A.; Hook, F.; Nylander, T.; Sparr, E., Assembly of RNA nanostructures on supported lipid bilayers. *Nanoscale* **2015,** *7* (2), 583-596.
36. Garnier, B.; Bouter, A.; Gounou, C.; Petry, K. G.; Brisson, A. R., Annexin A5-Functionalized Liposomes for Targeting Phosphatidylserine-Exposing Membranes. *Bioconjugate Chemistry* **2009,** *20* (11), 2114-2122.
37. Hellstrand, E.; Grey, M.; Ainalem, M.-L.; Ankner, J.; Forsyth, V. T.; Fragneto, G.; Haertlein, M.; Dauvergne, M.-T.; Nilsson, H.; Brundin, P.; Linse, S.; Nylander, T.; Sparr, E., Adsorption of α-Synuclein to Supported Lipid Bilayers: Positioning and Role of Electrostatics. *ACS Chemical Neuroscience* **2013,** *4* (10), 1339-1351.
38. Chen, Q.; Xu, S.; Liu, Q.; Masliyah, J.; Xu, Z., QCM-D study of nanoparticle interactions. *Advances in colloid and interface science* **2016,** *233*, 94-114.
39. Wu, L.; Jiang, X., Recent developments in methodology employed to study the interactions between nanomaterials and model lipid membranes. *Analytical and Bioanalytical Chemistry* **2015,** *408* (11), 2743-2758.
40. Arteta, M. Y.; Berti, D.; Montis, C.; Campbell, R. A.; Eriksson, C.; Clifton, L. A.; Skoda, M. W. A.; Soltwedel, O.; Koutsioubas, A.; Baglioni, P.; Nylander, T., On the formation of dendrimer/nucleolipids surface films for directed self-assembly. *Soft Matter* **2015,** *11* (10), 1973-1990.
41. Belicka, M.; Gerelli, Y.; Kucerka, N.; Fragneto, G., The component group structure of DPPC bilayers obtained by specular neutron reflectometry. *Soft Matter* **2015,** *11* (31), 6275-6283.

42. Kurniawan, J.; Kuhl, T. L., Characterization of Solid-Supported Dipalmitoylphosphatidylcholine Membranes Containing Cholesterol. *Langmuir* **2015,** *31* (8), 2527-2532.
43. Shen, H.-H.; Lake, V.; Le Brun, A. P.; James, M.; Duff, A. P.; Peng, Y.; McLean, K. M.; Hartley, P. G., Targeted detection of phosphatidylserine in biomimetic membranes and in vitro cell systems using annexin V-containing cubosomes. *Biomaterials* **2013,** *34* (33), 8361-8369.
44. Richter, R.; Mukhopadhyay, A.; Brisson, A., Pathways of Lipid Vesicle Deposition on Solid Surfaces: A Combined QCM-D and AFM Study. *Biophysical Journal* **2003,** *85* (5), 3035-3047.
45. Di Silvio, D.; Rigby, N.; Bajka, B.; Mayes, A.; Mackie, A.; Baldelli Bombelli, F., Technical tip: high-resolution isolation of nanoparticle-protein corona complexes from physiological fluids. *Nanoscale* **2015,** *7* (28), 11980-11990.
46. Sauerbrey, G., Verwendung von Schwingquarzen zur Wägung dünner Schichten und zur Mikrowägung. *Zeitschrift für Physik* **1959,** *155* (2), 206-222.
47. Cubitt, R.; Fragneto, G., D17: the new reflectometer at the ILL. *Applied Physics A* **2002,** *74* (1), 329-331.
48. Bayerl, T. M.; Thomas, R. K.; Penfold, J.; Rennie, A.; Sackmann, E., Specular reflection of neutrons at phospholipid monolayers. Changes of monolayer structure and headgroup hydration at the transition from the expanded to the condensed phase state. *Biophysical Journal* **1990,** *57* (5), 1095-1098.
49. Nagle, J. F.; Tristram-Nagle, S., Structure of lipid bilayers. *Biochimica et Biophysica Acta (BBA) - Reviews on Biomembranes* **2000,** *1469* (3), 159-195.
50. Caruso, F.; Möhwald, H., Protein Multilayer Formation on Colloids through a Stepwise Self-Assembly Technique. *Journal of the American Chemical Society* **1999,** *121* (25), 6039-6046.
51. Zwang, T. J.; Fletcher, W. R.; Lane, T. J.; Johal, M. S., Quantification of the Layer of Hydration of a Supported Lipid Bilayer. *Langmuir* **2010,** *26* (7), 4598-4601.
52. Vandoolaeghe, P.; Rennie, A. R.; Campbell, R. A.; Nylander, T., Neutron Reflectivity Studies of the Interaction of Cubic-Phase Nanoparticles with Phospholipid Bilayers of Different Coverage. *Langmuir* **2009,** *25* (7), 4009-4020.
53. Wiener, M. C.; White, S. H., Structure of a fluid dioleoylphosphatidylcholine bilayer determined by joint refinement of x-ray and neutron diffraction data. III. Complete structure. *Biophysical Journal* **1992,** *61* (2), 434-447.
54. Hristova, K.; White, S. H., Determination of the hydrocarbon core structure of fluid dioleoylphosphocholine (DOPC) bilayers by x-ray diffraction using specific bromination of the double-bonds: effect of hydration. *Biophysical Journal* **1998,** *74* (5), 2419-2433.
55. Kučerka, N.; Nagle, J. F.; Sachs, J. N.; Feller, S. E.; Pencer, J.; Jackson, A.; Katsaras, J., Lipid Bilayer Structure Determined by the Simultaneous Analysis of Neutron and X-Ray Scattering Data. *Biophysical Journal* **2008,** *95* (5), 2356-2367.
56. Negoda, A.; Kim, K.-J.; Crandall, E. D.; Worden, R. M., Polystyrene nanoparticle exposure induces ion-selective pores in lipid bilayers. *Biochimica et Biophysica Acta (BBA) - Biomembranes* **2013,** *1828* (9), 2215-2222.
57. Wei, X.; Jiang, W.; Yu, J.; Ding, L.; Hu, J.; Jiang, G., Effects of SiO2 nanoparticles on phospholipid membrane integrity and fluidity. *Journal of Hazardous Materials* **2015,** *287*, 217-224.
58. Montis, C.; Maiolo, D.; Alessandri, I.; Bergese, P.; Berti, D., Interaction of nanoparticles with lipid membranes: a multiscale perspective. *Nanoscale* **2014,** *6* (12), 6452-6457.

59. Le Brun, A. P.; Haigh, C. L.; Drew, S. C.; James, M.; Boland, M. P.; Collins, S. J., Neutron reflectometry studies define prion protein N-terminal peptide membrane binding. *Biophysical Journal* **2014,** *107* (10), 2313-2324.
60. Gonzalez-Rodriguez, D.; Barakat, A. I., Dynamics of Receptor-Mediated Nanoparticle Internalization into Endothelial Cells. *PLoS ONE* **2015,** *10* (4), e0122097.
61. Monopoli, M. P.; Walczyk, D.; Campbell, A.; Elia, G.; Lynch, I.; Baldelli Bombelli, F.; Dawson, K. A., Physical−Chemical Aspects of Protein Corona: Relevance to in Vitro and in Vivo Biological Impacts of Nanoparticles. *Journal of the American Chemical Society* **2011,** *133* (8), 2525-2534.